Available online at www.sciencedirect.com
ScienceDirect
Applied Mathematical Modelling 31 (2007) 18–37
APPLIED MATHEMATICAL MODELLING
www.elsevier.com/locate/apm

Mathematical simulation of a seven link biped robot on various surfaces and ZMP considerations

Peiman Naseradin Mousavi, Ahmad Bagheri *

Department of Mechanical Engineering, Guilan University, Rasht, Iran

Received 1 October 2005; received in revised form 1 June 2006; accepted 27 June 2006
Available online 1 September 2006

Abstract

In recent years, numerous researches have been done based on simulation of legged mechanism, especially on biped robots simulation and control. The following article focuses on the biped robot simulation and control over various manners such as horizontal, ascending and descending surfaces with the aid of mathematical modeling methods (in MATLAB/SIMULINK environment). Similar parameters to human walking process will be obtained such as ZMP and joint's actuator torques. The mathematical simulation has been used to interpolate trajectory of the robot path with the given break points. Of course, after the robot's path determination, third-order spline method will be used because of the very high precision and ability to calculate the kinematic and dynamic parameters. With the aid of this program, common parameters such as linear and angular velocity and acceleration, joint's angles and inertial forces for the given specifications and conditions (Nominal, no disturbances) will be calculated and simulated. Also, the two types of ZMP (Fixed and moving) have been considered and calculated with the aid of the software.

Keywords: Seven link biped robot; ZMP; Vandermonde matrix; Third-order spline; Trajectory interpolation; Simulation; Fixed and moving ZMP; Torso modified motion

1. Introduction

Recently, numerous collaborations have been focused on the biped robot walking pattern to trace the desired paths and perform the required tasks. Many researches such as dynamic analysis [1–5], and stability criterion [6,7] have been published. Zerrugh et al. [8] have considered biped robot with respect to walking pattern with the aid of recording human kinematic data. McGeer et al. [9] have focused on passive walking of the biped robot generated by gravity and inertia over a declined surface. Silva et al. [10] have focused on actuator power and energy by walking parameters regulation. Stability of the robot will appear upon the biped robot

* Corresponding author.
E-mail addresses: payman.mousavi@gmail.com, payman.mousavi@azarabenergy.com (P.N. Mousavi), Bagheri@guilan.ac.ir (A. Bagheri).

0307-904X/$ - see front matter © 2006 Published by Elsevier Inc.
doi:10.1016/j.apm.2006.06.018

intention to tip over. Zheng et al. [11] have considered a method of gait synthesis with respect to static stability while Chevallereau et al. [12] have focused on dynamic stability by a low energy reference trajectory definition. Takanishi et al. [13], Shih et al. [14], Hirai et al. [15], and Dasgupta et al. [16] have considered dynamic stability of the robot with respect to walking process based on the zero moment point (ZMP) method [6]. In the current article, with respect to the various conditions of the surfaces, Shih et al. [17,18], Huang et al., Yokoi et al., Kajita et al., Kaneko et al., Arai et al., Koyachi et al., and Tanie et al. [19] used methods to generate the trajectory paths of the robot have been used. The most impressive biped is ASIMO (Standing for Advanced Step in Innovation Mobility) developed by the Honda Corporation [20,21]. ASIMO is an autonomous three dimensional walker with 26-DOF weighing 43 kg and measuring 1.2 m in height and is capable of walking at 0.3 m/s on level ground and climbing and descending stairs. ASIMO's development began in the mid-1980s and continues to the present day. The development has involved ten generations of prototypes, named E0 through E6 and P1 through P3, and has cost tens of millions of dollars. Following Honda's success, the Japanese government began the Humanoid Robot Project (HRP) in an attempt to grow Japan's service robot. In this article, it has been focused on the used inverse kinematic and dynamic methods for providing the robot paths in order to obtain smooth motion of the robot. The used procedure avoids the link's velocity discontinuities of the robot in order to mitigate occurrence impact effects and also obtain suitable control process. Based on the explained process, the controlling system will produce optimum actuator torques with respect to minimum energy consumption. The main contribution of this work contains a new method for simulation of the seven link biped robot for providing a new environment of the biped walking. The process has been performed based on the system given break points and either third-order spline or Vandermonde Matrix interpolation method. The used methods generate the desired trajectory paths to avoid oscillation of the paths because of high order of polynomials. The simulations have been done for single and combined paths. Similar to human gait, the robot's foots make negative, zero and positive angles with the ground. The designed software has been used for the biped robot simulation which will present the needed robot parameters such as linear and angular velocity and acceleration of links, total inertial forces, joint's actuator torques, link's angle and ZMP. The software will present the simulated movies in the desired steps that are defined by the users. The software has significant properties such as simultaneous simulation of the robot over various surfaces.

Finally, obtaining the ZMP diagrams, the stability behavior of the robot can be judged easily. Also, the two types of ZMP (fixed and moving) and their advances have been considered.

2. Kinematic modeling

The inverse kinematic modeling of the robot needs direct usage of mathematical interpolation. The mathematical interpolation is one of the simplest methods used for providing the suitable curves with respect to the given break points that the system must undergo. The controlling system of biped robot needs to use kinematic equations to obtain the desired parameters, so it would be able to use them into the domain of dynamic and control relations. The process of inverse kinematic equations analysis with the aid of the presented and identified paths (they have been indicated by the operator) and also solving the nonlinear equations for the robot movement will result in the needed parameters. Parameters such as angles, velocities and accelerations of joints will be obtained for use in dynamic and the subsequent controlling equations before the actual calculation of the "Actuator Torques". The actuator torques will be used in the indicated paths. In the current article, the simplest mathematical interpolations which are "Vandermonde Matrix" and "Third-Order Spline" [17–19] have been used. This means for the calculation of the requested paths and influence of $(n+1)$ break points, either a polynomial of nth order or a third-order spline is needed. The mathematical equations of a biped robot are nonlinear systems of equations which contain complex mathematical relations. In Fig. 1, the robot saggital schematic has been presented to indicate the required nodes and the utility of the mentioned curves. With utilization of the specified criteria, the generated paths will be used in the designed software to obtain the kinematic parameters. In general and with respect to Fig. 1, all the needed and important robot parameters are listed as following:

(a) Hip parameters (hip joint)
(b) Foot parameters (ankle joint)

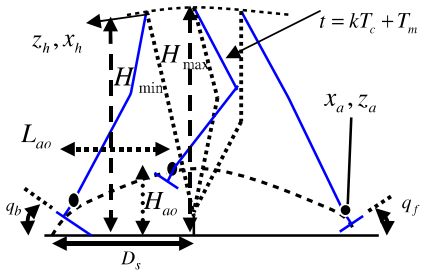

Fig. 1. The saggital configuration of biped robot and needed parameters for interpolation.

(a) Hip parameters:
The hip parameters include vertical and horizontal displacements of the joint (z_h, x_h) and the variables which are illustrated by Figs. 1 and 2 respectively. The distance between the hip and fixed coordinate system which is supposed to be on the support leg, will be denoted for the instants of the beginning and the end points of the double support phase by x_{ed}, x_{sd} respectively.

(b) Foot parameters:
During the walking cycle, the horizontal and vertical displacements of ankle joint are represented by x_a, z_a, respectively. The other parameters are listed as following:

T_c	total traveling time, including single and double support phases,
T_d	double support phase time, which it is regarded as 20% of T_c,
T_m	the time which ankle joint has reached maximum height during walking cycle,
k	step number,
H_{ao}	ankle joint maximum height,
L_{ao}	the horizontal traveled distance between ankle joint and start point when the ankle joint has reached its maximum height,
D_s	step length,
q_b, q_f	foot lift angle and contact angle with the level ground,
q_{gs}, q_{gf}	the ground initial terrain angles,
λ	surface slope,
h_{st}	stair level height,
H_{st}	foot maximum height from stair level.

Now, the main robot's parameters (hip and foot) will be considered for interpolation of the trajectory paths which lead to solve the nonlinear equations and obtain simulation parameters such as link's angles and subsequently kinematic and dynamic relations based on the obtained angles.

2.1. Foot trajectory interpolation

The foot parameters can be categorized into several cases as following:

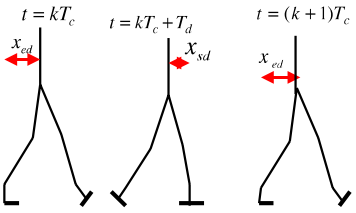

Fig. 2. The variables of hip: x_{ed}, x_{sd}.

2.1.1. Foot angle on horizontal surfaces or stair [19]

Both surfaces and stair use the same break points, as in Fig. 1, it can be written as below:

$$\theta_a(t) = \begin{cases} -q_{gs} & t = kT_c, \\ -q_b & t = kT_c + T_d, \\ q_f & t = (k+1)T_c, \\ q_{gf} & t = (k+1)T_c + T_d. \end{cases} \tag{1}$$

2.1.2. Foot angle on declined surfaces

Regarding Section 2.1.1, the following break points will be used:

$$\theta_a(t) = \begin{cases} (\lambda - q_{gs}) & t = kT_c, \\ \lambda - q_b & t = kT_c + T_d, \\ \lambda + q_f & t = (k+1)T_c, \\ \lambda + q_{gf} & t = (k+1)T_c + T_d. \end{cases} \tag{2}$$

Now, the above mentioned break points are used to calculate the trajectory paths. In the current process of the polynomial determination, boundary conditions of the movement play an important role for providing the trajectory paths.

The required boundary conditions are determined with respect to the system identity and requirements. Similar to human walking process, foot angular velocity ($\dot{\theta}_a$) at the specified moments including the instants of the beginning and the end of foot traveling is equal to zero:

$$\dot{\theta}_a[t = kT_c, t = kT_c + T_d] = 0. \tag{3}$$

With respect to relations (1) or (2) and (3), either a fourth-order polynomial or third-order spline can be used to obtain the foot trajectory. For the explained process, many short programs have been designed to calculate and present the trajectory simulations with the aid of the user's identified input data.

Similar processes are used to calculate the trajectory paths for the displacements of horizontal and vertical foot traveling. The obtained trajectory paths will be used for the biped robot simulation.

2.1.3. The displacements of horizontal and vertical foot traveling over horizontal surfaces [19] or stair

As can be seen in Figs. 1 and 3, the needed foot displacement relations for horizontal and vertical movements are written as following:

$$x_{ahor}(t) = \begin{cases} kD_s & t = kT_c, \\ kD_s + l_{an}\sin q_b + \cdots & t = kT_c + T_d, \\ l_{af}(1 - \cos q_b) & \\ kD_s + L_{ao} & t = kT_c + T_m, \\ (k+2)D_s - l_{an}\sin q_f - \cdots & t = (k+1)T_c, \\ l_{ab}(1 - \cos q_f) & \\ (k+2)D_s & t = (k+1)T_c + T_d, \end{cases} \tag{4}$$

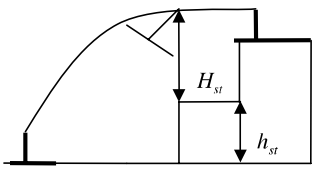

Fig. 3. The foot trajectory on stair and the required parameters.

$$z_{\mathrm{ahor}}(t)=\begin{cases} h_{\mathrm{gs}}+l_{\mathrm{an}} & t=kT_{\mathrm{c}},\\ h_{\mathrm{gs}}+l_{\mathrm{af}}\sin q_{\mathrm{b}}+l_{\mathrm{an}}\cos q_{\mathrm{b}} & t=kT_{\mathrm{c}}+T_{\mathrm{d}},\\ H_{\mathrm{ao}} & t=kT_{\mathrm{c}}+T_{\mathrm{m}},\\ h_{\mathrm{ge}}+l_{\mathrm{ab}}\sin q_{\mathrm{f}}+l_{\mathrm{an}}\cos q_{\mathrm{f}} & t=(k+1)T_{\mathrm{c}},\\ h_{\mathrm{ge}}+l_{\mathrm{an}} & t=(k+1)T_{\mathrm{c}}+T_{\mathrm{d}}, \end{cases} \tag{5}$$

$$z_{\mathrm{stair}}(t)=\begin{cases} (k-1)h_{\mathrm{st}}+l_{\mathrm{an}} & t=kT_{\mathrm{c}},\\ (k-1)h_{\mathrm{st}}+l_{\mathrm{af}}\sin q_{\mathrm{b}}+\cdots & t=kT_{\mathrm{c}}+T_{\mathrm{d}},\\ l_{\mathrm{an}}\cos q_{\mathrm{b}} & \\ kh_{\mathrm{st}}+H_{\mathrm{st}} & t=kT_{\mathrm{c}}+T_{\mathrm{m}},\\ (k+1)h_{\mathrm{st}}+l_{\mathrm{ab}}\sin q_{\mathrm{f}}+\cdots & t=(k+1)T_{\mathrm{c}},\\ l_{\mathrm{an}}\cos q_{\mathrm{f}} & \\ (k+1)h_{\mathrm{st}}+l_{\mathrm{an}} & t=(k+1)T_{\mathrm{c}}+T_{\mathrm{d}}. \end{cases} \tag{6}$$

2.1.4. The displacements of horizontal and vertical foot traveling over declined surfaces

In order to obtain the required trajectory paths for the needed foot movement on declined surfaces, the following relations are used:

$$x_{\mathrm{a,dec}}(t)=\begin{cases} kD_{\mathrm{s}}\cos\lambda-l_{\mathrm{an}}\sin\lambda & t=kT_{\mathrm{c}},\\ (kD_{\mathrm{s}}+l_{\mathrm{af}})\cos\lambda+\cdots & t=kT_{\mathrm{c}}+T_{\mathrm{d}},\\ l_{\mathrm{an}}\sin(q_{\mathrm{b}}-\lambda)-l_{\mathrm{af}}\cos(q_{\mathrm{b}}-\lambda) & \\ (kD_{\mathrm{s}}+L_{\mathrm{ao}})\cos\lambda & t=kT_{\mathrm{c}}+T_{\mathrm{m}},\\ ((k+2)D_{\mathrm{s}}-l_{\mathrm{ab}})\cos\lambda-\cdots & t=(k+1)T_{\mathrm{c}},\\ l_{\mathrm{an}}\sin(q_{\mathrm{f}}+\lambda)+l_{\mathrm{ab}}\cos(q_{\mathrm{f}}+\lambda) & \\ (k+2)D_{\mathrm{s}}\cos\lambda-l_{\mathrm{an}}\sin\lambda & t=(k+1)T_{\mathrm{c}}+T_{\mathrm{d}}, \end{cases} \tag{7}$$

$$z_{\mathrm{a,dec}}(t)=\begin{cases} kD_{\mathrm{s}}\sin\lambda+l_{\mathrm{an}}\cos\lambda & t=kT_{\mathrm{c}},\\ (kD_{\mathrm{s}}+l_{\mathrm{af}})\sin\lambda+\cdots & t=kT_{\mathrm{c}}+T_{\mathrm{d}},\\ +l_{\mathrm{an}}\cos(q_{\mathrm{b}}-\lambda)+l_{\mathrm{af}}\sin(q_{\mathrm{b}}-\lambda) & \\ (kD_{\mathrm{s}}+L_{\mathrm{ao}})\sin\lambda+H_{\mathrm{ao}}\cos\lambda & t=kT_{\mathrm{c}}+T_{\mathrm{m}},\\ ((k+2)D_{\mathrm{s}}-l_{\mathrm{ab}})\sin\lambda+\cdots & t=(k+1)T_{\mathrm{c}},\\ l_{\mathrm{an}}\sin(q_{\mathrm{f}}+\lambda)+l_{\mathrm{ab}}\cos(\pi/2-(q_{\mathrm{f}}+\lambda)) & \\ (k+2)D_{\mathrm{s}}\sin\lambda+l_{\mathrm{an}}\cos\lambda & t=(k+1)T_{\mathrm{c}}+T_{\mathrm{d}}. \end{cases} \tag{8}$$

Particularly, the following domain boundary conditions must be applied with respect to the biped movement for the above mentioned break points:

$$\begin{cases} \dot{\theta}_{\mathrm{a}}(kT_{\mathrm{c}})=0,\\ \dot{\theta}_{\mathrm{a}}((k+1)T_{\mathrm{c}}+T_{\mathrm{d}})=0, \end{cases}$$

$$\begin{cases} \dot{x}_{\mathrm{a}}(kT_{\mathrm{c}})=0,\\ \dot{x}_{\mathrm{a}}((k+1)T_{\mathrm{c}}+T_{\mathrm{d}})=0, \end{cases}$$

$$\begin{cases} \dot{z}_{\mathrm{a}}(kT_{\mathrm{c}})=0,\\ \dot{z}_{\mathrm{a}}((k+1)T_{\mathrm{c}}+T_{\mathrm{d}})=0, \end{cases}$$

2.1.5. Hip trajectory interpolation for the level ground [19] and declined surfaces

As can be seen in Fig. 2, the needed hip break points must be determined from the following:

$$x_{\mathrm{h,Hor.stair}} = \begin{cases} kD_{\mathrm{s}} + x_{\mathrm{ed}} & t = kT_{\mathrm{c}}, \\ (k+1)D_{\mathrm{s}} - x_{\mathrm{sd}} & t = kT_{\mathrm{c}} + T_{\mathrm{d}}, \\ (k+1)D_{\mathrm{s}} + x_{\mathrm{ed}} & t = (k+1)T_{\mathrm{c}}, \end{cases} \tag{9}$$

$$x_{\mathrm{h,Dec.}} = \begin{cases} (kD_{\mathrm{s}} + x_{\mathrm{ed}})\cos\lambda & t = kT_{\mathrm{c}}, \\ ((k+1)D_{\mathrm{s}} - x_{\mathrm{sd}})\cos\lambda & t = kT_{\mathrm{c}} + T_{\mathrm{d}}, \\ ((k+1)D_{\mathrm{s}} + x_{\mathrm{ed}})\cos\lambda & t = (k+1)T_{\mathrm{c}}, \end{cases} \tag{10}$$

$$z_{\mathrm{h,Hor.}} = \begin{cases} H_{\mathrm{hmin}} & t = kT_{\mathrm{c}}, \\ H_{\mathrm{hmax}} & t = kT_{\mathrm{c}} + .5(T_{\mathrm{c}} - T_{\mathrm{d}}), \\ H_{\mathrm{hmin}} & t = (k+1)T_{\mathrm{c}}, \end{cases} \tag{11}$$

$$z_{\mathrm{h,Dec.}} = \begin{cases} H_{\mathrm{hmin}}\cos\lambda + \cdots & t = kT_{\mathrm{c}}, \\ (kD_{\mathrm{s}} + x_{\mathrm{ed}})\sin\lambda & \\ H_{\mathrm{hmax}}\cos\lambda + \cdots & t = kT_{\mathrm{c}} + 5(T_{\mathrm{c}} - T_{\mathrm{d}}), \\ + (kD_{\mathrm{s}} + x_{\mathrm{sd}})\sin\lambda & \\ H_{\mathrm{hmin}}\cos\lambda + \cdots & t = (k+1)T_{\mathrm{c}}, \\ ((k+1)D_{\mathrm{s}} + x_{\mathrm{ed}})\sin\lambda, & \end{cases} \tag{12}$$

$$z_{\mathrm{stair}} = \begin{cases} (k-1)h_{\mathrm{s}} + H_{\mathrm{hmin}} & t = kT_{\mathrm{c}}, \\ kh_{\mathrm{s}} + H_{\mathrm{hmax}} & t = kT_{\mathrm{c}} + .5(T_{\mathrm{c}} - T_{\mathrm{d}}), \\ kh_{\mathrm{s}} + H_{\mathrm{hmin}} & t = (k+1)T_{\mathrm{c}}, \end{cases} \tag{13}$$

where, H_{hmin}, H_{hmax} are the hip minimum and maximum heights measured from the fixed coordinate system. Using the above mentioned relations and also utilization of the designed programs, the desired trajectory paths of the robot for the selected surfaces will be obtained with respect to each user's given input data. The simulation results are presented in Section 4. Now, the kinematic parameters will be obtained with respect to the above mentioned trajectory paths combined with the domain of the nonlinear equations (see Fig. 4).

The nonlinear equations can be written as below:

For support legs:

$$\begin{aligned} &l_1\cos(\pi - \theta_1) + l_2\cos(\pi - \theta_2) = a, \\ &l_1\sin(\pi - \theta_1) + l_2\sin(\pi - \theta_2) = b. \end{aligned} \tag{14}$$

For swing legs:

$$\begin{aligned} &l_3\cos(\theta_3) + l_4\cos(\theta_4) = c, \\ &l_3\sin(\theta_3) + l_4\sin(\theta_4) = d, \end{aligned} \tag{15}$$

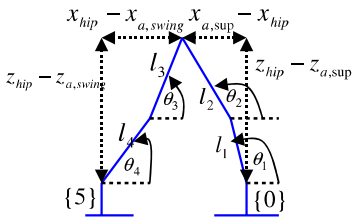

Fig. 4. The link's angles and configuration.

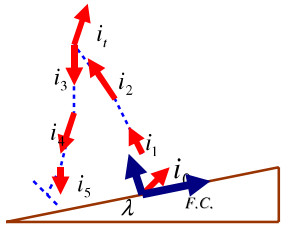

Fig. 5. The assumed unit vectors to obtain position vectors.

which,

$$a = x_{\mathrm{a,Sup}} - x_{\mathrm{hip}},$$
$$b = z_{\mathrm{hip}} - z_{\mathrm{a,Sup}},$$
$$c = x_{\mathrm{hip}} - x_{\mathrm{a,swing}},$$
$$d = z_{\mathrm{hip}} - z_{\mathrm{a,swing}}.$$

With the aid of the written programs, the mentioned nonlinear equations based on the gait parameters are solved and also the link's angles will be obtained. The relations of Appendix A are used to extract the kinematic variables. As shown in Fig. 5, the robot kinematic relations can be provided easily. Using simplest rigid body's configuration and also assuming the fixed coordinate system (FCS) on edge of the support foot, the position vector of links with respect to the fixed coordinate system are obtained as can be found in Appendix A.

3. Dynamic investigations

Similar to human gait, the important stability criteria is so called "ZMP". The ZMP is a point on the ground whose sum of all moments around this point is equal to zero. The ZMP formula is written as following [19]:

$$x_{\mathrm{zmp}} = \frac{\sum_{i=1}^{n} m_i(g\cos\lambda + \ddot{z}_i)x_i - \sum_{i=1}^{n} m_i(g\sin\lambda + \ddot{x}_i)z_i - \sum_{i=1}^{n} {}^{i}I_i\ddot{\theta}_i}{\sum_{i=1}^{n} m_i(g\cos\lambda + \ddot{z}_i)},$$

where $\ddot{x}_i$, $\ddot{z}_i$ are mass center's vertical and horizontal acceleration of link (i) with respect to the fixed coordinate system. $\ddot{\theta}_i$ is angular acceleration of link (i) obtained from the interpolation process and λ denotes the slope of the surface. Mainly, the two types of ZMP are considered as following:

(a) Moving ZMP
(b) Fixed ZMP

The moving type of the robot walking is similar to human gait. In the fixed type, the ZMP position is restricted through the support feet or the user's selected areas. Consequently, the significant torso's modified motion is required for stable walking of the robot. For the explained process, the software has been designed to find target angle of the torso for providing the fixed ZMP position automatically. In the designed software, q_{torso} shows the deflection angle of the torso determined by the user or calculated by auto detector mood of the software. Note, in the mood of auto detector, the torso needed motion for obtaining the mentioned fixed ZMP will be extracted with respect to the desired ranges. The desired ranges include the defined support feet area by the users or automatically by the designed software. Note, the most affecting parameters for obtaining the robot's stable walking are the hip's height and position. By varying the parameters with iterative method for x_{ed}, x_{sd} [19] and choosing the optimum hip height, the robot control process with respect to the torso's

modified angles and the mentioned parameters can be performed. To obtain the joint's actuator torques, the Lagrangian relation [22] has been used at the single support phase as below:

$$\tau_i = H(q)\ddot{q} + C(q,\dot{q})\dot{q} + G(q_i),$$

where, $i = 0, 2, \ldots, 6$ and H, C, G are mass inertia, coriolis and gravitational matrices of the system which can be written as following:

$$H(q) = \begin{bmatrix} h_{11} & h_{12} & h_{13} & h_{14} & h_{15} & h_{16} & h_{17} \\ h_{21} & h_{22} & h_{23} & h_{24} & h_{25} & h_{26} & h_{27} \\ h_{31} & h_{32} & h_{33} & h_{34} & h_{35} & h_{36} & h_{37} \\ h_{41} & h_{42} & h_{43} & h_{44} & h_{45} & h_{46} & h_{47} \\ h_{51} & h_{52} & h_{53} & h_{54} & h_{55} & h_{56} & h_{57} \\ h_{61} & h_{62} & h_{63} & h_{64} & h_{65} & h_{66} & h_{67} \end{bmatrix} \quad C(q,\dot{q}) = \begin{bmatrix} c_{11} & c_{12} & c_{13} & c_{14} & c_{15} & c_{16} & c_{17} \\ c_{21} & c_{22} & c_{23} & c_{24} & c_{25} & c_{26} & c_{27} \\ c_{31} & c_{32} & c_{33} & c_{34} & c_{35} & c_{36} & c_{37} \\ c_{41} & c_{42} & c_{43} & c_{44} & c_{45} & c_{46} & c_{47} \\ c_{51} & c_{52} & c_{53} & c_{54} & c_{55} & c_{56} & c_{57} \\ c_{61} & c_{62} & c_{63} & c_{64} & c_{65} & c_{66} & c_{67} \end{bmatrix} \quad G(q) = \begin{bmatrix} G_1 \\ G_2 \\ G_3 \\ G_4 \\ G_5 \\ G_{\text{tor}} \end{bmatrix}$$

The most important point in the double support phase of the biped walking is the used modified equation with respect to occurrence impact between the swing leg and the ground [23–25]. The simplification of the shown components of the matrices are complex and bulk mathematical functions and can be found in the given reference [26].

Below, two components of mass inertia matrix are presented. Note, the extracted components will be used in control process which can be found in the given reference [26].

$$\begin{aligned} h_{11} = {} & [m_1(l_{c1}^2 + l_{c1} l_e \cos(q_1 - \varphi))] + [m_2(l_1^2 + l_{c2}^2 + l_1 l_e \cos(q_1 - \varphi) + l_{c2} l_e \cos(q_2 - \varphi) + 2 l_1 l_{c2} \cos(q_2 - q_1))] \\ & + [m_3(l_1^2 + l_2^2 + l_{c3}^2 + l_1 l_e \cos(q_1 - \varphi) + l_2 l_e \cos(q_2 - \varphi) - l_{c3} l_e \cos(-q_3 + \varphi) + 2 l_1 l_2 \cos(q_2 - q_1) \\ & - 2 l_1 l_{c3} \cos(q_1 - q_3) - 2 l_2 l_{c3} \cos(q_2 - q_3))] + [m_4(l_1^2 + l_2^2 + l_3^2 + l_{c4}^2 + l_1 l_e \cos(q_1 - \varphi) + l_2 l_e \cos(q_2 - \varphi) \\ & - l_3 l_e \cos(q_3 - \varphi) - l_{c4} l_e \cos(-q_4 + \varphi) + 2 l_1 l_2 \cos(q_2 - q_1) - 2 l_1 l_3 \cos(q_3 - q_1) - 2 l_1 l_{c4} \cos(q_1 - q_4) \\ & - 2 l_2 l_3 \cos(q_3 - q_2) - 2 l_2 l_{c4} \cos(q_2 - q_4) + 2 l_{c4} l_3 \cos(q_3 - q_4))] + [m_5(l_1^2 + l_2^2 + l_3^2 + l_4^2 + l_{\text{cfswing}}^2 \\ & + l_1 l_e \cos(q_1 - \varphi) + l_2 l_e \cos(q_2 - \varphi) - l_3 l_e \cos(q_3 - \varphi) - l_4 l_e \cos(q_4 - \varphi) - l_{\text{cfswing}} l_e \cos(\varphi - (\pi/2) \\ & + q_{\text{fswing}} - \beta_{\text{fswing}}) + 2 l_1 l_2 \cos(q_2 - q_1) - 2 l_1 l_3 \cos(q_3 - q_1) - 2 l_1 l_4 \cos(q_4 - q_1) - 2 l_1 l_{\text{cfswing}} \cos(q_1 - (\pi/2) \\ & + q_{\text{fswing}} - \beta_{\text{fswing}}) - 2 l_2 l_3 \cos(q_3 - q_2) - 2 l_2 l_4 \cos(q_4 - q_2) - 2 l_2 l_{\text{cfswing}} \cos(q_2 - (\pi/2) + q_{\text{fswing}} - \beta_{\text{fswing}}) \\ & + 2 l_3 l_4 \cos(q_4 - q_3) + 2 l_4 l_{\text{cfswing}} \cos(q_4 - (\pi/2) + q_{\text{fswing}} - \beta_{\text{fswing}}) + 2 l_3 l_{\text{cfswing}} \cos(q_3 - (\pi/2) \\ & + q_{\text{fswing}} - \beta_{\text{fswing}})] + [m_{\text{tor}}(l_1^2 + l_2^2 + l_{\text{ctorso}}^2 + l_1 l_e \cos(q_1 - \varphi) + l_2 l_e \cos(q_2 - \varphi) \\ & + l_e l_{\text{ctorso}} \cos(-q_{\text{torso}} - \varphi - (\pi/2)) + 2 l_1 l_2 \cos(q_2 - q_1) + 2 l_1 l_{\text{ctorso}} \cos(-q_{\text{torso}} - q_1 - (\pi/2)) \\ & + 2 l_2 l_{\text{ctorso}} \cos(q_{\text{torso}} + q_2 + (\pi/2))] + I_1 + I_2 + I_3 + I_4 + I_5 + I_{\text{torso}}, \end{aligned}$$

$$\begin{aligned} h_{21} = {} & [m_2(l_{c2}^2 + l_{c2} l_e \cos(q_2 - \varphi) + l_1 l_{c2} \cos(q_2 - q_1))] + [m_3(l_2^2 + l_{c3}^2 + l_2 l_e \cos(q_2 - \varphi) - l_{c3} l_e \cos(-q_3 + \varphi) \\ & + l_1 l_2 \cos(q_2 - q_1) - l_1 l_{c3} \cos(q_1 - q_3) - 2 l_2 l_{c3} \cos(q_2 - q_3))] + [m_4(l_2^2 + l_3^2 + l_{c4}^2 + l_2 l_e \cos(q_2 - \varphi) \\ & - l_3 l_e \cos(q_3 - \varphi) - l_{c4} l_e \cos(-q_4 + \varphi) + l_1 l_2 \cos(q_2 - q_1) - l_1 l_3 \cos(q_3 - q_1) - l_1 l_{c4} \cos(q_1 - q_4) \\ & - 2 l_2 l_3 \cos(q_3 - q_2) - 2 l_2 l_{c4} \cos(q_2 - q_4) + 2 l_{c4} l_3 \cos(q_3 - q_4))] + [m_5(l_2^2 + l_3^2 + l_4^2 + l_{\text{cfswing}}^2 + l_2 l_e \cos(q_2 - \varphi) \\ & - l_3 l_e \cos(q_3 - \varphi) - l_4 l_e \cos(q_4 - \varphi) - l_{\text{cfswing}} l_e \cos(\varphi - (\pi/2) + q_{\text{fswing}} - \beta_{\text{fswing}}) + l_1 l_2 \cos(q_2 - q_1) \\ & - l_1 l_3 \cos(q_3 - q_1) - l_1 l_4 \cos(q_4 - q_1) - l_1 l_{\text{cfswing}} \cos(q_1 - (\pi/2) + q_{\text{fswing}} - \beta_{\text{fswing}}) - 2 l_2 l_3 \cos(q_3 - q_2) \\ & - 2 l_2 l_4 \cos(q_4 - q_2) - 2 l_2 l_{\text{cfswing}} \cos(q_2 - (\pi/2) + q_{\text{fswing}} - \beta_{\text{fswing}}) + 2 l_3 l_4 \cos(q_4 - q_3) + 2 l_4 l_{\text{cfswing}} \cos(q_4 - (\pi/2) \\ & + q_{\text{fswing}} - \beta_{\text{fswing}}) + 2 l_3 l_{\text{cfswing}} \cos(q_3 - (\pi/2) + q_{\text{fswing}} - \beta_{\text{fswing}}))] + [m_{\text{tor}}(l_2^2 + l_{\text{ctorso}}^2 + l_2 l_e \cos(q_2 - \varphi) \\ & + l_e l_{\text{ctorso}} \cos(-q_{\text{torso}} - \varphi - (\pi/2)) + l_1 l_2 \cos(q_2 - q_1) + l_1 l_{\text{ctorso}} \cos(-q_{\text{torso}} - q_1 - (\pi/2)) + 2 l_2 l_{\text{ctorso}} \cos(q_{\text{torso}} + q_2 \\ & + (\pi/2))] + I_2 + I_3 + I_4 + I_5 + I_{\text{torso}}, \end{aligned}$$

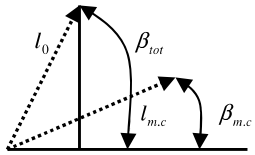

Fig. 6. The foot parameter.

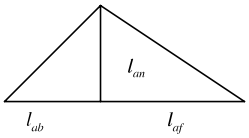

Fig. 7. The foot configuration.

where,

$$\varphi = q_{\mathrm{f}} + \beta_{\mathrm{m\cdot c}} + \lambda,$$

which, $\beta_{\mathrm{m\cdot c}}$, β_{tot} are presented in Fig. 6 and $\beta_{\mathrm{s,m\cdot c}}$ shows the angle of the swing foot's mass center measured from the fixed coordinate system.

With respect to the above mentioned relations, the designed software can simulate the seven link biped robot over various manners simultaneously. Also, one can obtain the kinematic and dynamic parameters such as the joint's actuator torques and the link's inertial forces for the two types of the ZMP (moving and fixed). The mentioned parameters can be seen in the simulation results.

4. Simulation results

In the designed software, the mentioned simulation processes for the two types of ZMP have been used for both of the nominal and un-nominal gait. For the un-nominal walking of the robot, the hip parameters (hip height) have been changed to consider the effects of the un-nominal motion upon the joint's actuator torques. The results are presented in Figs. 8–14 while the robot walks over declined surfaces for the single phase of the walking. Fig. 15 shows combined path of the robot. The used specifications of the simulation of the robot are listed in Table 1. Figs. 8, 10 and 12 display the moving type of ZMP with the nominal walking of the robot. Figs. 9, 11 and 13 show the same type of ZMP and also the un-nominal walking of the robot (with the changed hip height form the fixed coordinate system). Fig. 14 shows the fixed ZMP upon descending surface. As can been seen from the table, the swing and support legs have the same geometrical and inertial values whereas in the designed software the users can choose different specifications. Note, the swing leg impact and the ground has been regarded in the designed software as given in references [23–25]. Below, the saggital movement and stability analysis of the seven link biped robot has been considered whereas the frontal considerations are neglected. For convenience, 3D simulations of the biped robot are presented. In Table 1, l_{an}, l_{ab} and l_{af} present the foot profile which are displayed in Fig. 7.

5. Conclusion

The presented article focuses on the mathematical interpolation of the seven link biped robot (for both of the ZMP). The explained designed software process (12,000 lines) simulates the biped robot over various manners. The software enables the user to compare the results as presented in figures, the paths for the single phase walking of the robot have been concerned. In the software with the aid of the given break points, either

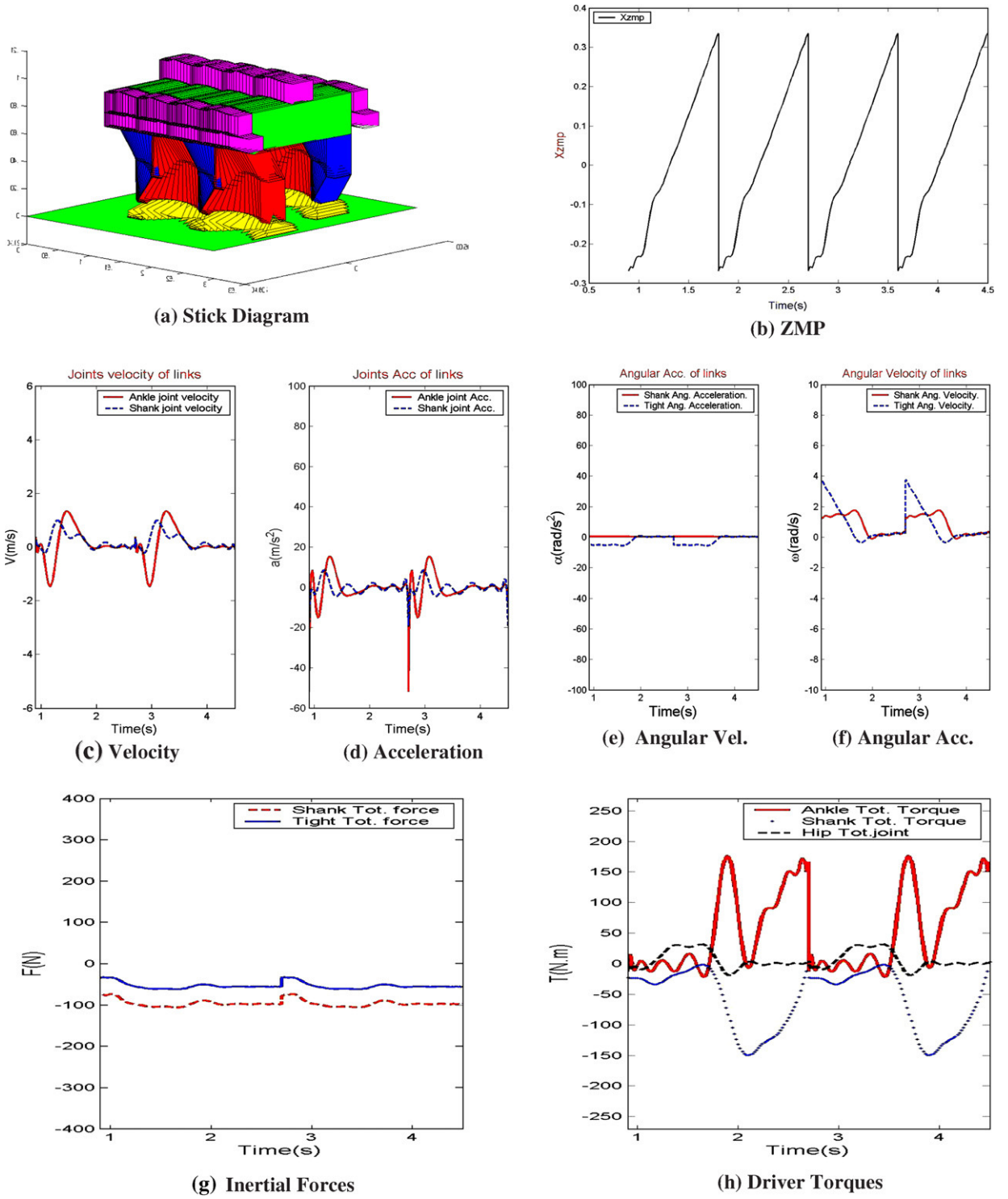

Fig. 8. (a) The robot's stick diagram on $\lambda = 0°$, Moving ZMP, $H_{min} = 0.60$ m, $H_{max} = 0.62$ m, (b) the moving ZMP diagram in nominal gait which satisfies stability criteria, (c) (—) shank MC velocity, (---) tight MC velocity, (d) (—) shank MC acceleration, (---) tight MC acceleration, (e) (—) shank angular velocity, (---) tight angular velocity, (f) (—) shank angular acceleration, (---) tight angular acceleration, (g) (—) shank MC inertial force, (---) tight MC inertial force, (h) (—) ankle joint torque, (---) hip joint torque, (...) shank joint torque.

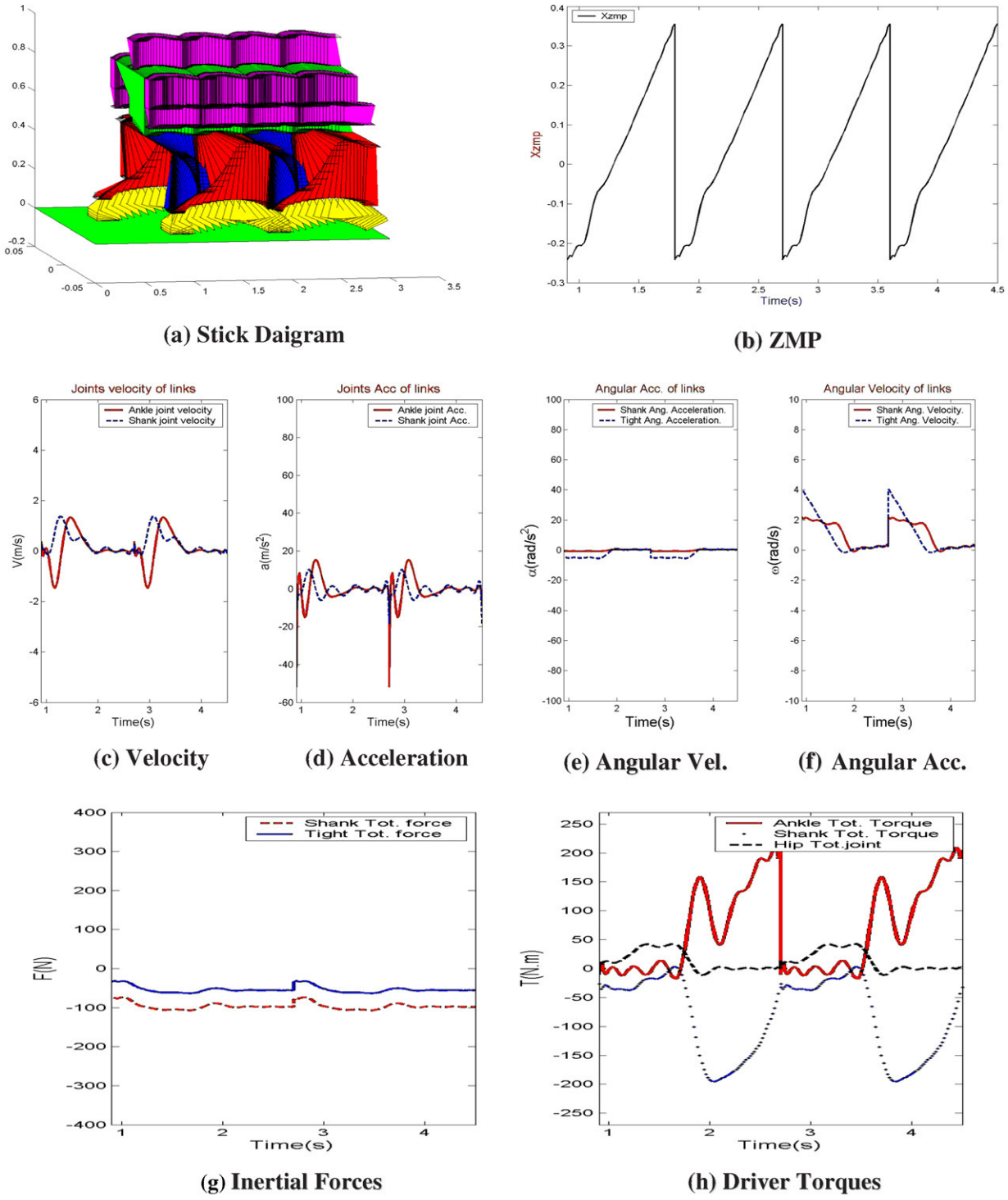

Fig. 9. (a) The robot's stick diagram on $\lambda = 0°$, moving ZMP, $H_{min} = 0.50$ m, $H_{max} = 0.52$ m, (b) the moving ZMP diagram in nominal gait which satisfies stability criteria, (c) (—) shank MC velocity, (---) tight MC velocity, (d) (—) shank MC acceleration, (---) tight MC acceleration, (e) (—) shank angular velocity, (---) tight angular velocity, (f) (—) shank angular acceleration, (---) tight angular acceleration, (g) (—) shank MC inertial force, (---) tight MC inertial force, (h) (—) ankle joint torque, (---) hip joint torque, (. . .) shank joint torque.

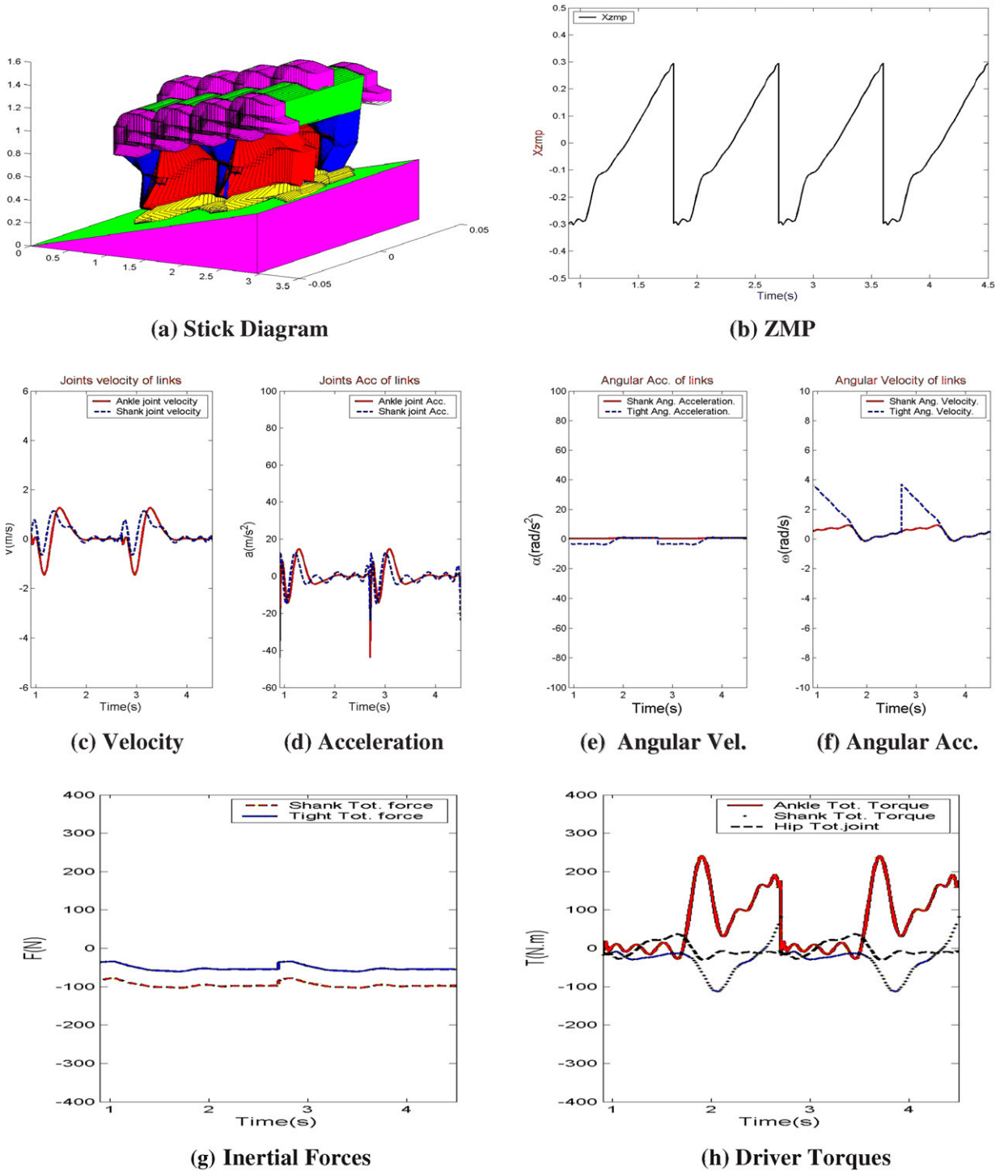

Fig. 10. (a) The robot's stick diagram on $\lambda = 10°$, moving ZMP, $H_{min} = 0.60$ m, $H_{max} = 0.62$ m, (b) the moving ZMP diagram in nominal gait which satisfies stability criteria, (c) (—) shank MC velocity, (---) tight MC velocity, (d) (—) shank MC acceleration, (---) tight MC acceleration, (e) (—) shank angular velocity, (---) tight angular velocity, (f) (—) shank angular acceleration, (---) tight angular acceleration, (g) (—) shank MC inertial force, (---) tight MC inertial force, (h) (—) ankle joint torque, (---) hip joint torque, (...) shank joint torque.

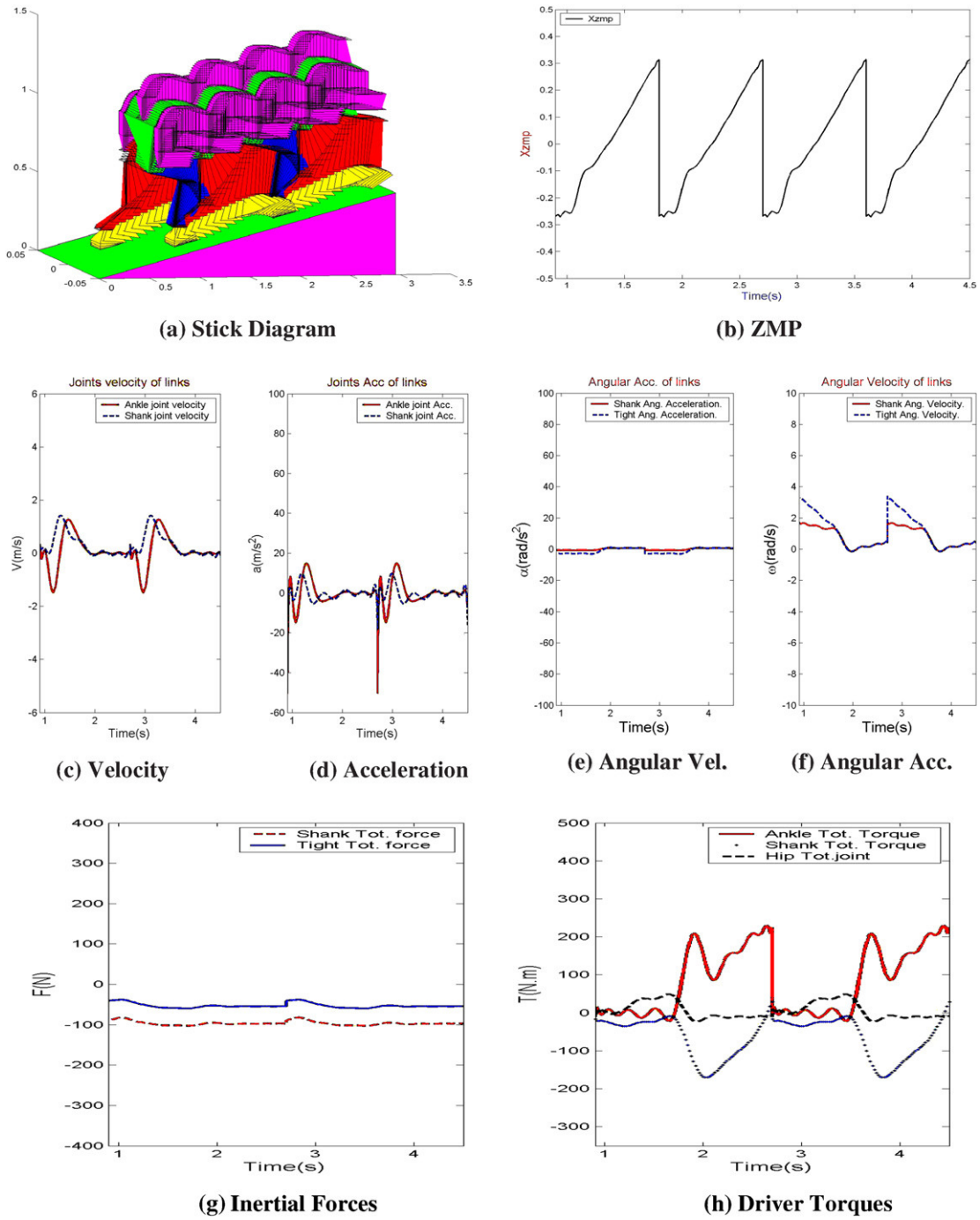

Fig. 11. (a) The robot's stick diagram on $\lambda = 10°$, Moving ZMP, $H_{min} = 0.50$ m, $H_{max} = 0.52$ m, (b) the moving ZMP diagram in nominal gait which satisfies stability criteria, (c) (—) shank MC velocity, (---) tight MC velocity, (d) (—) shank MC acceleration, (---) tight MC acceleration, (e) (—) shank angular velocity, (---) tight angular velocity, (f) (—) shank angular acceleration, (---) tight angular acceleration, (g) (—) shank MC inertial force, (---) tight MC inertial force, (h) (—) ankle joint torque, (---) hip joint torque, (. . .) shank joint torque.

third-order spline or Vandermonde Matrix has been used for providing the different trajectory paths. With the aid of the designed software, the kinematic, dynamic and control parameters have been evaluated. Also, the

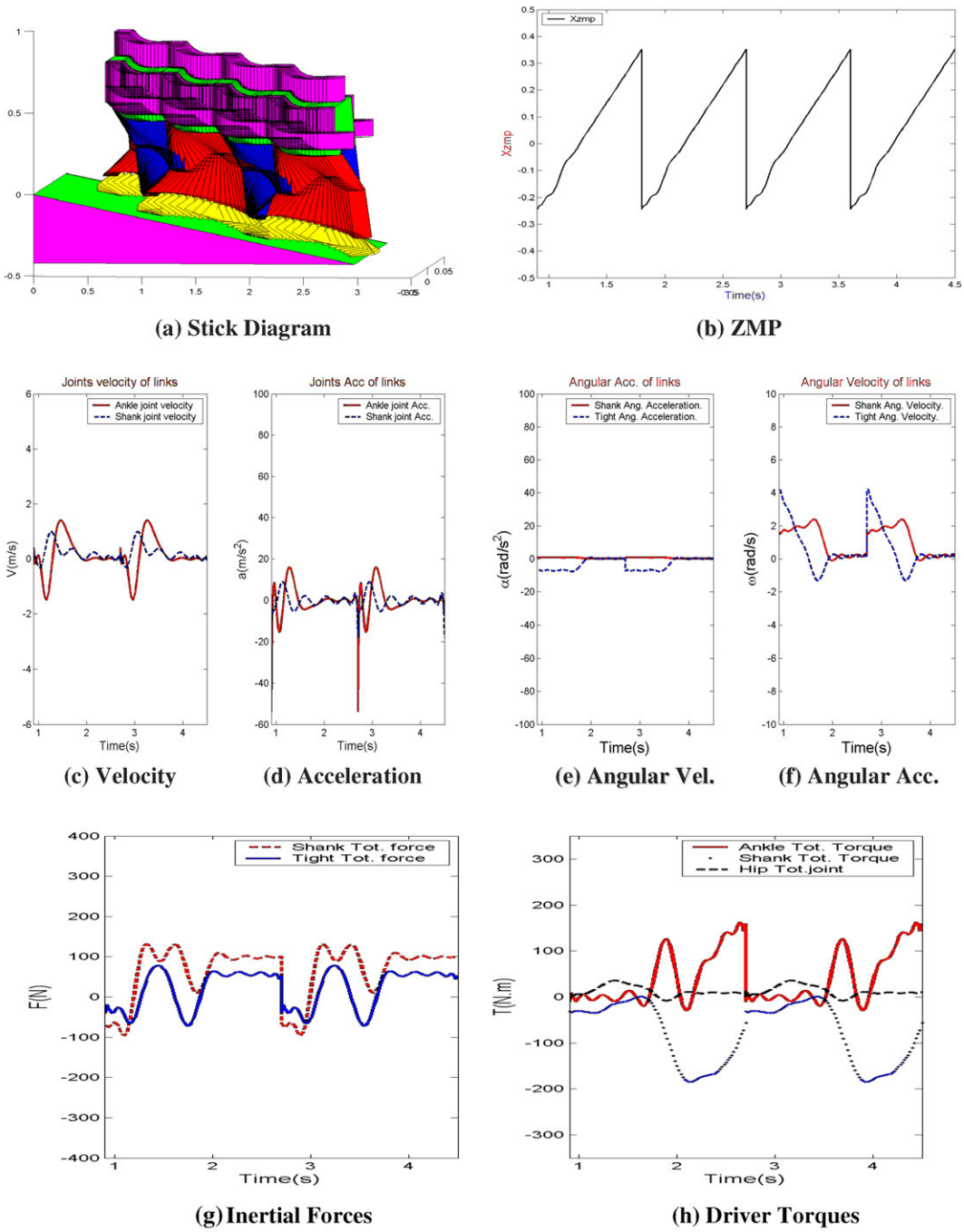

Fig. 12. (a) The robot's stick diagram on $\lambda = -8°$, moving ZMP, $H_{min} = 0.60$ m, $H_{max} = 0.62$ m, (b) the moving ZMP diagram in nominal gait which satisfies stability criteria, (c) (—) shank MC velocity, (---) tight MC velocity, (d) (—) shank MC acceleration, (---) tight MC acceleration, (e) (—) shank angular velocity, (---) tight angular velocity, (f) (—) shank angular acceleration, (---) tight angular acceleration, (g) (—) shank MC inertial force, (---) tight MC inertial force, (h) (—) ankle joint torque, (---) hip joint torque, (...) shank joint torque.

two types of ZMP have been investigated. The presented simulations indicate the hip height effects over joint's actuator torques for minimizing energy consumption and especially obtaining fine stability margin. As can be

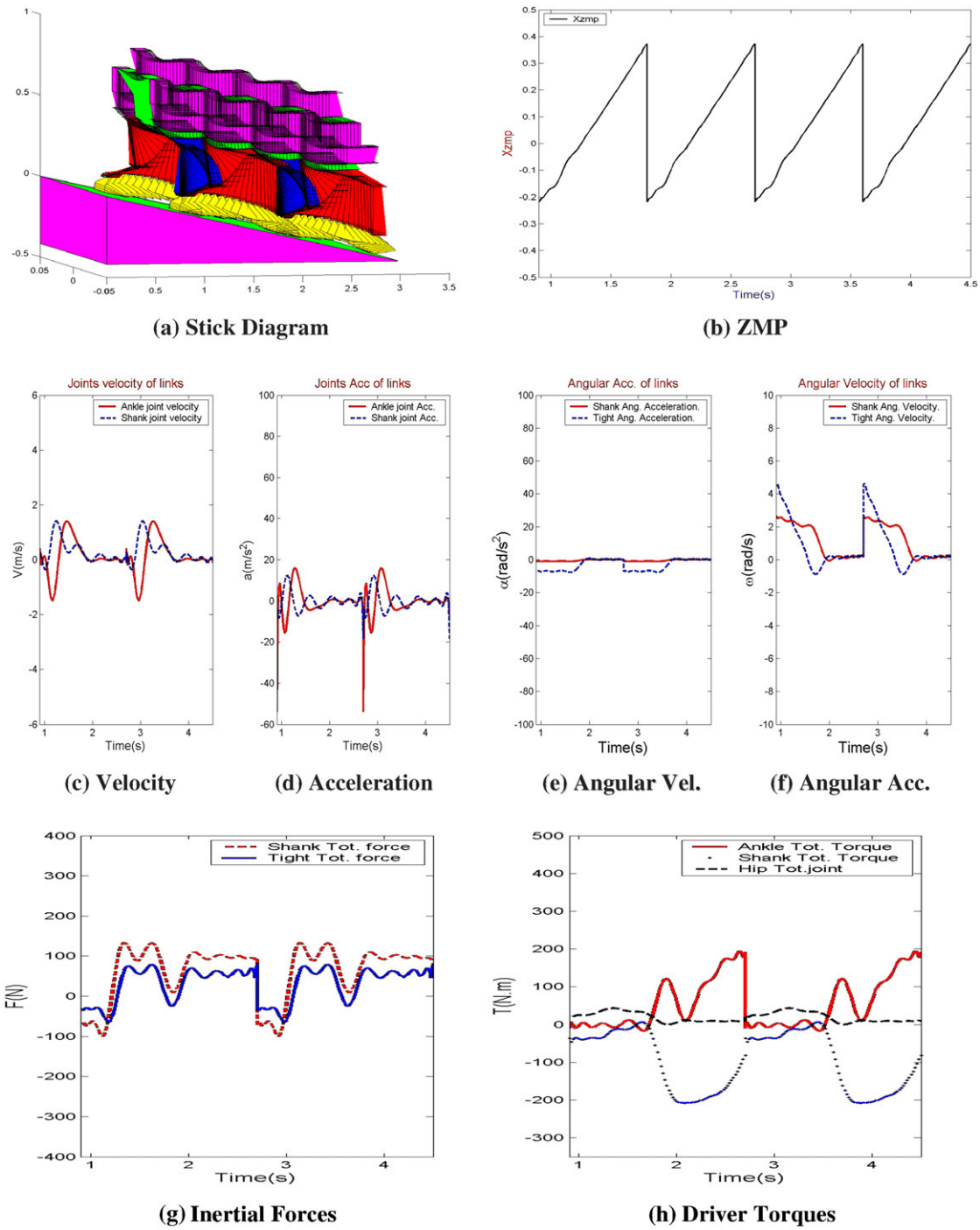

Fig. 13. (a) The robot's stick diagram on $\lambda = -8°$, Moving ZMP, $H_{min} = 0.50$ m, $H_{max} = 0.52$ m, (b) the moving ZMP diagram in nominal gait which satisfies stability criteria, (c) (—) shank MC velocity, (---) tight MC velocity, (d) (—) shank MC acceleration, (---) tight MC acceleration, (e) (—) shank angular velocity, (---) tight angular velocity, (f) (—) shank angular acceleration, (---) tight angular acceleration, (g) (—) shank MC inertial force, (---) tight MC inertial force, (h) (—) ankle joint torque, (---) hip joint torque, (. . .) shank joint torque.

seen in Figs. 9(h), 11(h) and 13(h), for the un-nominal walking of the robot with the lower hip height, the knee's actuator torque values is more than the obtained values as shown in Figs. 8(h), 10(h) and 12(h)

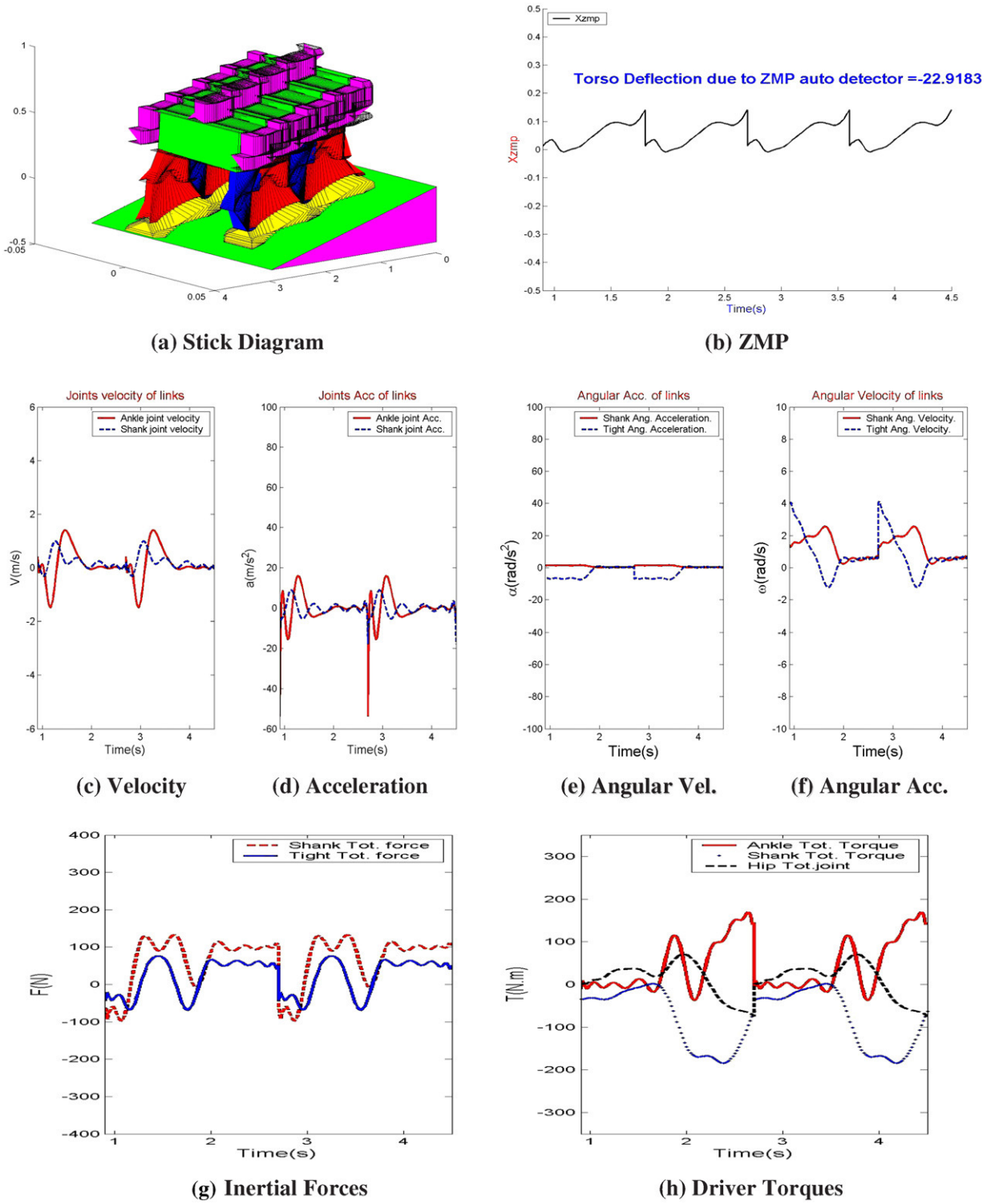

Fig. 14. (a) The robot's stick diagram on $\lambda = -8°$, fixed ZMP, $H_{min} = 0.60$ m, $H_{max} = 0.62$ m, (b) the fixed ZMP diagram in nominal gait which satisfies stability criteria, (c) (—) shank MC velocity, (---) tight MC velocity, (d) (—) shank MC acceleration, (---) tight MC acceleration, (e) (—) shank angular velocity, (---) tight angular velocity, (f) (—) shank angular acceleration, (---) tight angular acceleration, (g) (—) shank MC inertial force, (---) tight MC inertial force, (h) (—) ankle joint torque, (---) hip joint torque, (...) shank joint torque.

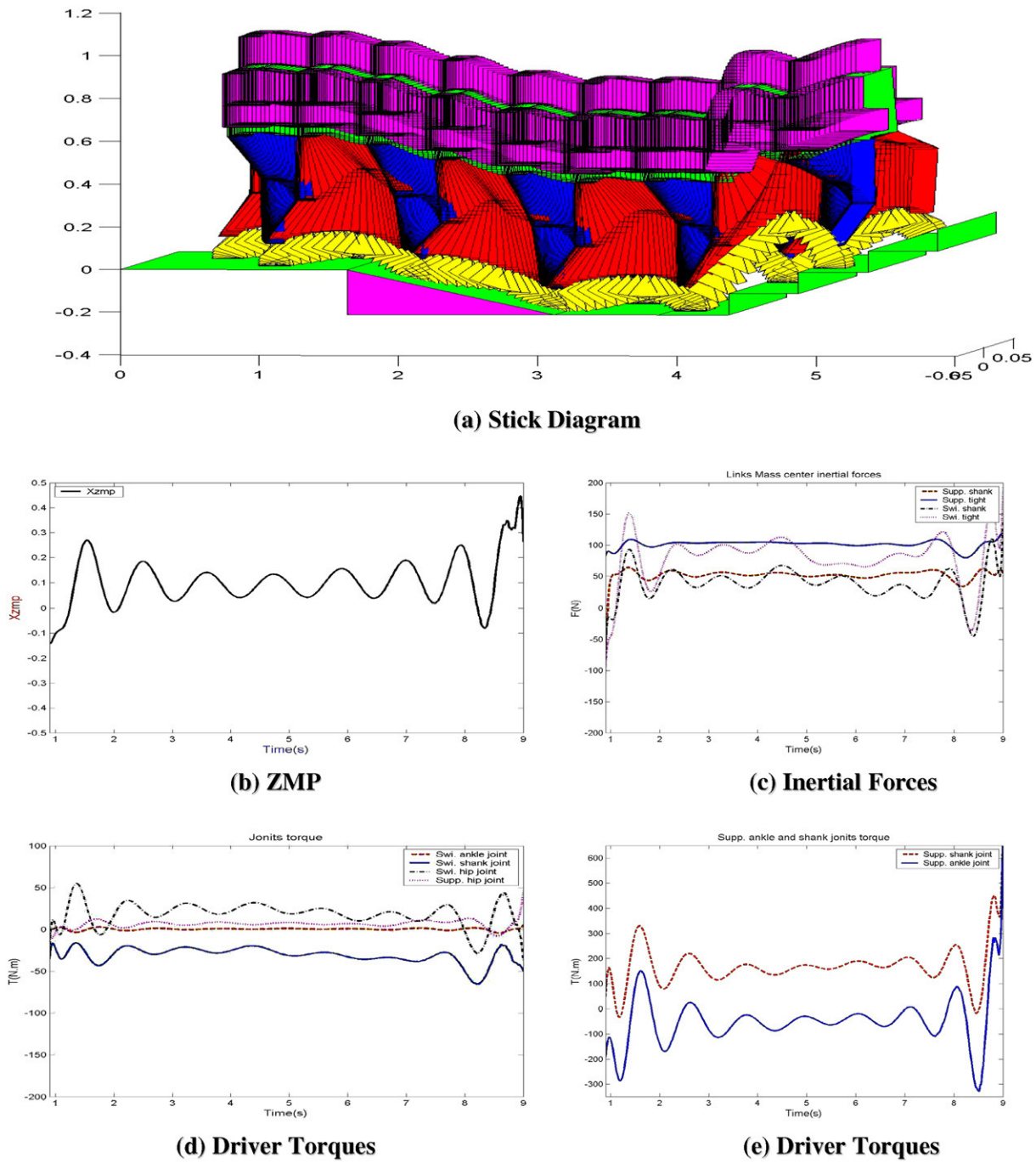

Fig. 15. (a) The robot's stick diagram on combined surface, nominal motion, moving ZMP, $\lambda = -8°$, (b) the moving ZMP diagram in nominal gait which satisfies stability criteria, (c) inertial forces (—) Supp. tight, (---) Supp. shank, (. . .) swing tight, ·-·- swing shank, (d) joint's torques (—) swing shank joint, (---) swing ankle joint, (. . .) Supp. hip joint, ·-·- swing hip joint, (e) joint's torques (—) Supp. ankle joint, (---) Supp. shank joint.

(for the nominal gait with the higher hip height). This is due to the robot's need to bend its knee joint more at a low hip position. Therefore, the large knee joint torque is required to support the robot. Therefore, for reducing the load on the knee joint and consequently with respect to minimum energy consumption, it is essential to keep the hip at a high position. Finally, the trajectory path generation needs more precision with respect to the

Table 1
The simulated robot specifications

$l_{Sh.}$	$l_{Ti.}$	$l_{To.}$	l_{an}	l_{ab}	l_{af}
0.3 m	0.3 m	0.3 m	0.1 m	0.1 m	0.13 m
$m_{Sh.}$	$m_{Th.}$	$m_{To.}$	$m_{Fo.}$	D_s	T_c
5.7 kg	10 kg	43 kg	3.3 kg	0.5 m	0.9 s
T_d	T_m	H_{ao}	L_{ao}	x_{ed}	x_{sd}
0.18 s	0.4 s	0.16 m	0.4 m	0.23 m	0.23 m
g_{gs}	g_{gf}	H_{min}	H_{max}	h_s	H_s
0	0	0.60 m	0.62 m	0.1 m	0.15 m

I_{shank}	I_{tight}	I_{torso}	I_{foot}
0.02 kg m^2	0.08 kg m^2	1.4 kg m^2	0.01 kg m^2

obtained kinematic relations to avoid the link's velocity discontinuities. The presented results have an acceptable consistency with the typical robot.

Acknowledgement

We wish to express our sincere thanks to the many who made the successful completion of this work possible, especially my holy colleague Mr. Ahmad Arjomandkhah for his talent and guidance.

Appendix A

The position vectors of the links, linear velocities and accelerations with respect to the fixed coordinate system are written as below:

Position vectors

$$\vec{r}_0 = l_{m\cdot c}(\cos(\beta_{m\cdot c} + q_f)I + \sin(\beta_{m\cdot c} + q_f)K), \tag{1}$$

$$\vec{r}_1 = (l_0\cos(\beta_{tot} + q_f) + l_{c1}\cos(\theta_1 - \lambda))I + (l_{c1}\sin(\theta_1 - \lambda) + l_0\sin(\beta_{tot} + q_f))K, \tag{2}$$

$$\vec{r}_2 = (l_0\cos(\beta_{tot} + q_f) + l_1\cos(\theta_1 - \lambda) - l_{c2}\cos(\pi - \theta_2 + \lambda))I + (l_1\sin(\theta_1 - \lambda) + l_0\sin(\beta_{tot} + q_f) + l_{c2}\sin(\pi - \theta_2 + \lambda))K, \tag{3}$$

$$\vec{r}_3 = (l_0\cos(\beta_{tot} + q_f) + l_1\cos(\theta_1 - \lambda) - l_2\cos(\pi - \theta_2 + \lambda) - l_{c3}\cos(\theta_3 - \lambda))I + (l_1\sin(\theta_1 - \lambda) + l_0\sin(\beta_{tot} + q_f) + l_2\sin(\pi - \theta_2 + \lambda) - l_{c3}\sin(\theta_3 - \lambda))K, \tag{4}$$

$$\vec{r}_4 = (l_0\cos(\beta_{tot} + q_f) + l_1\cos(\theta_1 - \lambda) - l_2\cos(\pi - \theta_2 + \lambda) - l_3\cos(\theta_3 - \lambda) - l_{c4}\cos(\theta_4 - \lambda))I + (l_1\sin(\theta_1 - \lambda) + l_0\sin(\beta_{tot} + q_f) + l_2\sin(\pi - \theta_2 + \lambda) - l_3\sin(\theta_3 - \lambda) - l_{c4}\sin(\theta_4 - \lambda))K, \tag{5}$$

$$\vec{r}_5 = (l_0\cos(\beta_{tot} + q_f) + l_1\cos(\theta_1 - \lambda) - l_2\cos(\pi - \theta_2 + \lambda) - l_3\cos(\theta_3 - \lambda) - l_4\cos(\theta_4 - \lambda) - l_{5m\cdot c}\cos(\pi/2 - \lambda + \beta_{s,m.s} - q_b))I + (l_1\sin(\theta_1 - \lambda) + l_0\sin(\beta_{tot} + q_f) + l_2\sin(\pi - \theta_2 + \lambda) - l_3\sin(\theta_3 - \lambda) - l_4\sin(\theta_4 - \lambda) - l_{5m\cdot c}\sin(\pi/2 - \lambda + \beta_{s,m.s} - q_b)))K, \tag{6}$$

$$\begin{aligned}\vec{r}_{\text{tor}} = {} & (l_0\cos(\beta_{\text{tot}}+q_{\text{f}})+l_1\cos(\theta_1-\lambda)\\ & -l_2\cos(\pi-\theta_2+\lambda)+l_{\text{tor}}\cos(\pi/2-\theta_{\text{tor}}-\lambda))I\\ & +(l_1\sin(\theta_1-\lambda)+l_0\sin(\beta_{\text{tot}}+q_{\text{f}})\\ & +l_2\sin(\pi-\theta_2+\lambda)+l_{\text{tor}}\sin(\pi/2-\theta_{\text{tor}}-\lambda))K,\end{aligned} \tag{7}$$

Linear velocity:

$$\vec{v}_0 = l_{\text{m·c}}\vec{\omega}_0(-\sin(\beta_{\text{m·c}}+q_{\text{f}})I+\cos(\beta_{\text{m·c}}+q_{\text{f}})K), \tag{8}$$

$$\begin{aligned}\vec{v}_1 = {} & (-l_0\vec{\omega}_0\sin(\beta_{\text{tot}}+q_{\text{f}})-l_{\text{c1}}\vec{\omega}_1\sin(\theta_1-\lambda))I\\ & +(l_{\text{c1}}\vec{\omega}_1\cos(\theta_1-\lambda)+l_0\cos(\beta_{\text{tot}}+q_{\text{f}}))K,\end{aligned} \tag{9}$$

$$\begin{aligned}\vec{v}_2 = {} & (-l_0\vec{\omega}_0\sin(\beta_{\text{tot}}+q_{\text{f}})-l_1\vec{\omega}_1\sin(\theta_1-\lambda)\\ & -l_{\text{c2}}\vec{\omega}_2\sin(\pi-\theta_2+\lambda))I+(l_1\vec{\omega}_1\cos(\theta_1-\lambda)\\ & +l_0\vec{\omega}_0\cos(\beta_{\text{tot}}+q_{\text{f}})-l_{\text{c2}}\vec{\omega}_2\cos(\pi-\theta_2+\lambda))K,\end{aligned} \tag{10}$$

$$\begin{aligned}\vec{v}_3 = {} & (-l_0\vec{\omega}_0\sin(\beta_{\text{tot}}+q_{\text{f}})-l_1\vec{\omega}_1\sin(\theta_1-\lambda)\\ & -l_2\vec{\omega}_2\sin(\pi-\theta_2+\lambda)+l_{\text{c3}}\vec{\omega}_3\sin(\theta_3-\lambda))I\\ & +(l_1\vec{\omega}_1\cos(\theta_1-\lambda)+l_0\vec{\omega}_0\cos(\beta_{\text{tot}}+q_{\text{f}})\\ & -l_2\vec{\omega}_2\cos(\pi-\theta_2+\lambda)-l_{\text{c3}}\vec{\omega}_3\cos(\theta_3-\lambda))K,\end{aligned} \tag{11}$$

$$\begin{aligned}\vec{v}_4 = {} & (-l_0\vec{\omega}_0\sin(\beta_{\text{tot}}+q_{\text{f}})-l_1\vec{\omega}_1\sin(\theta_1-\lambda)\\ & -l_2\vec{\omega}_2\sin(\pi-\theta_2+\lambda)+l_3\vec{\omega}_3\sin(\theta_3-\lambda)\\ & +l_{\text{c4}}\vec{\omega}_4\sin(\theta_4-\lambda))I+(l_1\vec{\omega}_1\cos(\theta_1-\lambda)\\ & +l_0\vec{\omega}_0\cos(\beta_{\text{tot}}+q_{\text{f}})-l_2\vec{\omega}_2\cos(\pi-\theta_2+\lambda)\\ & -l_3\vec{\omega}_3\cos(\theta_3-\lambda)-l_{\text{c4}}\vec{\omega}_4\cos(\theta_4-\lambda))K,\end{aligned} \tag{12}$$

$$\begin{aligned}\vec{v}_5 = {} & (-l_0\vec{\omega}_0\sin(\beta_{\text{tot}}+q_{\text{f}})-l_1\vec{\omega}_1\sin(\theta_1-\lambda)\\ & -l_2\vec{\omega}_2\sin(\pi-\theta_2+\lambda)+l_3\vec{\omega}_3\sin(\theta_3-\lambda)\\ & +l_4\vec{\omega}_4\sin(\theta_4-\lambda)-l_{5\text{m·c}}\vec{\omega}_5\sin(\pi/2-\lambda+\beta_{\text{s,m·c}}-q_{\text{b}}))I\\ & +(l_1\vec{\omega}_1\cos(\theta_1-\lambda)+l_0\vec{\omega}_0\cos(\beta_{\text{tot}}+q_{\text{f}})\\ & -l_2\vec{\omega}_2\cos(\pi-\theta_2+\lambda)-l_3\vec{\omega}_3\cos(\theta_3-\lambda)\\ & -l_4\vec{\omega}_4\cos(\theta_4-\lambda)+l_{5\text{m·c}}\vec{\omega}_5\cos(\pi/2-\lambda+\beta_{\text{s,m·c}}-q_{\text{b}}))K,\end{aligned} \tag{13}$$

$$\begin{aligned}\vec{v}_{\text{tor}} = {} & (-l_0\vec{\omega}_0\sin(\beta_{\text{tot}}+q_{\text{f}})-l_1\vec{\omega}_1\sin(\theta_1-\lambda)\\ & -l_2\vec{\omega}_2\sin(\pi-\theta_2+\lambda)+l_{\text{tor}}\vec{\omega}_{\text{tor}}\sin(\pi/2-\theta_{\text{tor}}-\lambda))I\\ & +(\vec{\omega}_1 l_1\cos(\theta_1-\lambda)+l_0\vec{\omega}_0\cos(\beta_{\text{tot}}+q_{\text{f}})\\ & -l_2\vec{\omega}_2\cos(\pi-\theta_2+\lambda)-l_{\text{tor}}\vec{\omega}_{\text{tor}}\cos(\pi/2-\theta_{\text{tor}}-\lambda))K,\end{aligned} \tag{14}$$

Linear acceleration: Differentiating from relations (8)–(14), the link's acceleration vectors can be obtained easily.

References

[1] J. Fursho, M. Masubuchi, A theoretically motivated reduced order model for the control of dynamic biped locomotion, J. Dyn. Syst., Measure., Contr. DSMC-109 (1987) 155–163.
[2] S. Kajita, A. Kobayashi, T. Yamamura, Dynamic walking control of a biped robot along a potential energy conserving orbit, IEEE Trans. Robot. Automat. 8 (Aug) (1992) 431–438.
[3] W.T. Miller, A.L. Kun, Dynamic balance of a biped walking robot, in: Neural System for Robotics, Academic, New York, 1997, pp. 17–35.
[4] M. Garica, A. Chatterjee, A. Ruina, Speed, efficiency, and stability of small-slope 2-D passive dynamic bipedal walking, in: Proc. IEEE Int. Conf. Robotics and Automation, 1998, pp. 2351–2356.
[5] J.H. Park, H.A. Chung, Hybrid control for biped robots using impedance control and computed-torque control, in: Proc. IEEE Int. Conf. Robotics and Automation, 1999, pp. 1365–1370.

[6] M. Vukobratovic, D. Juricic, Contribution to the synthesis of biped gait, IEEE Trans. Bio-Med. Eng. BME-16 (1) (1969) 1–6.
[7] F. Gubina, H. Hemami, R.B. McGhee, On the dynamic stability of biped locomotion, IEEE Trans. Bio-Med. Eng. BME-21 (2) (1974) 102–108.
[8] M.Y. Zarrugh, C.W. Radcliffe, Computer generation of human gait kinematics, J. Biomech. 12 (1979) 99–111.
[9] T. McGeer, Passive walking with knees, in: Proc. IEEE Int. Conf. Robotics and Automation, 1990, pp. 1640–1645.
[10] F.M. Silva, J.A.T. Machado, Energy analysis during biped walking, in: Proc. IEEE Int. Conf. Robotics and Automation, 1999, pp. 59–64.
[11] Y.F. Zheng, J. Shen, Gait synthesis for the SD-2 biped robot to climb sloping surface, IEEE Trans. Robot. Automat. 6 (February) (1990) 86–96.
[12] C. Chevallereau, A. Formal'sky, B. Perrin, Low energy cost reference trajectories for a biped robot, in: Proc. IEEE Int. Conf. Robotics and Automation, 1998, pp. 1398–1404.
[13] A. Takanishi, M. Ishida, Y. Yamazaki, I. Kato, The realization of dynamic walking robot WL-10RD, in: Proc. Int. Conf. Advanced Robotics, 1985, pp. 459–466.
[14] C.L. Shih, Y.Z. Li, S. Churng, T.T. Lee, W.A. Cruver, Trajectory synthesis and physical admissibility for a biped robot during the single support phase, in: Proc. IEEE Int. Conf. Robotics and Automation, 1990, pp. 1646–1652.
[15] K. Hirai, M. Hirose, Y. Haikawa, T. Takenaka, The development of honda humanoid robot, in: Proc. IEEE Int. Conf. Robotics and Automation, 1998, pp. 1321–1326.
[16] A. Dasgupta, Y. Nakamura, Making feasible walking motion of humanoid robots from human motion capture data, in: Proc. IEEE Int. Conf. Robotics and Automation, 1999, pp. 1044–1049.
[17] C. Shih, Gait synthesis for a biped robot, Robotica 15 (1997) 599–607.
[18] Ascending and descending stairs for a biped robot, IEEE Trans. Syst., Man., Cybern. A 29 (3) (1999).
[19] Q. Huang, K. Yokoi, S. Kajita, K. Kaneko, H. Arai, N. Koyachi, K. Tanie, Planning walking patterns for a biped robot, IEEE Trans. Robot. Automat. 17 (3) (2001).
[20] Honda Corporation, ASIMO, Available from: <http://world.honda.com/ASIMO/>.
[21] K. Hirai, M. Hirose, Y. Haikawa, T. Takenake, The development of Honda humanoid robot, in: Proc. of the IEEE International Conference on Roboitcs and Automation, Leuven, Belgium, May 1998, pp. 1321–1326.
[22] J.G. John, Introduction to Robotics: Mechanics and Control, Addison-Wesley, 1989.
[23] H.K. Lum, M. Zribi, Y.C. Soh, Planning and contact of a biped robot, Int. J. Eng. Sci. 37 (1999) 1319–1349.
[24] Eric R. Westervelt, Toward a coherent framework for the control of planar biped locomotion, a dissertation submitted in partial fulfillment of the requirements for the degree of doctor of philosophy, (Electrical Engineering Systems), In the University of Michigan, 2003.
[25] H. Hon, T. Kim, T. Park, Tolerance analysis of a Spur gear train, in: Proc. 3rd DADS Korean user's Conf., 1978, pp. 61–81.
[26] P.N. Mousavi, Adaptive Control of 5 DOF Biped Robot Moving On A Declined Surface, MS Thesis, Guilan University, 2006.